Anisotropic flux pinning in $YBa_2Cu_3O_{7-\delta}$ single crystals: The influence of defect size and density as determined from neutron irradiation

F. M. Sauerzopf
Atominstitut der Österreichischen Universitäten, A-1020 Vienna, Austria
(Received 3 November 1997)

Substantial information about the pinning of flux lines in $YBa_2Cu_3O_{7-\delta}$ single crystals can be gained from an interpretation of the changes in the critical temperature T_c and the magnetization loops after neutron irradiation. After annealing the irradiated samples, a well-defined defect structure prevails. A careful interpretation of the data allows one to arrive at conclusions on the unknown defect structure and flux pinning before irradiation and annealing. The variation of T_c is explained by the mobility of smaller defects and their interaction with the radiation-induced defect cascades. The results on the critical current densities lead to the proposition that strong pinning prevails in most $YBa_2Cu_3O_{7-\delta}$ single crystals, even in the as-grown state. Current theories for the summation of the elementary pinning forces are tested, but cannot consistently explain the experimentally observed macroscopic pinning force. If the field is applied perpendicular to the crystallographic c axis, a significant influence of the smaller defects on the anisotropy of the crystal can be deduced from an analysis of the critical current densities. [S0163-1829(98)02817-3]

I. INTRODUCTION

Neutron irradiation has been used for a long time to enhance flux pinning in superconductors. In addition to this application-oriented approach, the method yielded substantial information on the mechanisms of flux pinning in low-T_c superconductors.[1,2] Soon after the discovery of high-T_c superconductors, a significant influence of particle irradiation on their properties was discovered.[3] Especially fast neutron-induced defects in single crystals of $YBa_2Cu_3O_{7-\delta}$ (YBCO) cause a huge increase of the critical currents. Subsequently the defect structure after neutron irradiation was examined by transmission electron microscopy (TEM), and spherical defects with a size of a few nm were identified,[4] the typical defect cascade regions. The size of these defects is comparable to the coherence length of the high-T_c superconductors (HTSC's) at elevated temperatures. Therefore, they create a perfect situation for core pinning, the dominant process for flux pinning in these materials. Consequently the interpretation of the experimental data was based on the effect of these large defects.[5,6] Very little is known about the nature and density of smaller defects, which are invisible to TEM. Especially the role of point defects and defect clusters was widely discussed, which have been shown to increase pinning substantially after electron[7] and proton irradiation[8,9] of YBCO. These types of radiation do not produce significant amounts of defect cascades, and the data were interpreted in terms of collective pinning.[10] The mobility of point defects strongly depends on temperature, which led to attempts to separate the contributions of small and large defects by annealing at various temperatures. Point defects in the oxygen sublattice are rather mobile even at room temperature. This stimulated an experiment, where a YBCO single crystal was irradiated at 4.2 K, then stored and measured without warming it above 90 K.[11] This left the irradiation-induced defect structure intact. Only after warming up to room temperature was the mobility of oxygen point defects restored. The resulting ''room-temperature annealing'' led to a reduction of the observed critical currents ($H\|c$) by about 10–20 %. Complementary experiments at Argonne National Laboratory considered critical currents after ambient temperature (reactor) irradiation and subsequent annealing of YBCO single crystals up to 300 °C.[9,12] This leads to a removal of smaller and less stable defects, while the defect cascades remain intact, as shown by TEM.[4] Also, at these temperatures no oxygen is lost from the crystal, but the mobility of the point defects is dramatically enhanced. The authors of this study found a reduction of $J_c^{ab;H\|c}$ (the critical current density in the ab planes with the field applied parallel to the crystallographic c direction, $H_a\|c$) by about 20%, and concluded that the dominating contribution to $J_c^{ab;H\|c}$ was due to the large defect cascades. The data on magnetization measurements for H_a perpendicular to the c direction yield $J_c^{c;H\|ab}$. The radiation-induced enhancement of this current density was almost completely removed after annealing, which led the authors to assume that the critical currents in that field orientation were not caused by the defect cascades. The question why defect cascades should effectively pin flux lines in one crystal direction, but not in the other, remained unanswered. In the following, an attempt to clear up the discrepancies was made by developing a qualitative model for the influence of the crystal anisotropy on flux pinning.[6] This model considers the joint influence of the layered structure and the anisotropy of the order parameter on flux pinning. It will be discussed and refined throughout the present paper. One basic feature is the possibility that pinning centers may be turned ineffective for $H_a\|ab$ by the very small order parameter between the CuO_2 planes, where the flux-line cores are situated due to the intrinsic pinning effect. There, the magnitude of the order parameter is a function of the material anisotropy, which in turn is affected by the anisotropy of the coupling strength and that of the properties of the charge carriers. Therefore, the strength of flux pinning of a given defect for $H\|ab$ may be influenced by changing the anisot-

ropy of the material. This can, for example, be achieved by removing or introducing small defects, which smear out the anisotropy of the Fermi surface by isotropic scattering of the electrons (cf. the theoretical approach[13]). The obvious need for a further clarification of the role of small defects for flux pinning led to a new set of experiments. In the present paper, a study of flux pinning after sequential annealing and neutron irradiation of one YBCO single crystal is presented. The density of small defects is considered to be characterized by the critical temperature T_c, and the anisotropic flux-pinning properties are evaluated from magnetization measurements with the field applied along the two main crystallographic directions, $H_a \| c$ and $H_a \| ab$. From this series of experiments the contributions of small and large defects can be distinguished, because the concentration of large defects accumulates after each irradiation step, while smaller defects are removed by the intermediate annealing. The results give evidence for the strong interaction between the defect structure in the as-grown crystal and the irradiation induced defects, and support our model of anisotropic flux pinning. They show, quite in contrast to expectation, a dominating influence of the TEM-invisible defects (either smaller than $\sim$1 nm, or structurally indistinguishable) on flux pinning for $H_a \| c$ at low neutron fluences, and a significant contribution of the defect cascades, if the field is applied perpendicular to the crystallographic c axis. In this case, also a significant contribution of the intrinsic pinning effect is found. An analysis of the dependence of the critical current densities for $H_a \| c$ on the induction B and the defect density will show that pinning in all sample states, even in the as-grown sample, is due to strong pinning, i.e., the pinning centers cause relatively large distortions of the flux-line lattice (FLL).

II. EXPERIMENTAL DETAILS

The crystal ($0.77 \times 0.76 \times 0.22$ mm^3, 0.813 mg) used in this experiment was grown by the self-flux method[14] and selected from a number of single crystals from similar batches by choosing the one with the smallest hysteresis at 77 K and at the same time a rather high T_c.[15] It is heavily twinned, with a twin boundary spacing of about 20 μm. The crystal quality is best characterized by the very low $J_c^{ab;H\|c}$ at 77 K, where the hysteresis loop is almost reversible. Granularity of the crystal can be ruled out from the comparison of the magnetization slopes in the Meissner state and after field reversal at 7.9 T.

In order to obtain reproducible results from the magnetic measurements, especially for $H_a \| ab$, the orientation of the crystal with respect to the field had to be accurately controlled. This was achieved by glueing the crystal to a larger sample holder (see Ref. 6 for details), from which it is never removed during the experiments. This sample holder is then inserted into the actual sample rod of the magnetometer, ensuring a reproducibility of better than 0.3°, which is vital for experiments with $H_a \| ab$. Vacuum grease was chosen as the glue, because it is very temperature stable up to 250 °C in air and not harmful to YBCO single crystals under our annealing conditions, as proved in separate experiments.[16] Actually, the limitation of the annealing temperature to 250 °C in air is a consequence of these tests. This does not significantly influence the results of the annealing process compared to annealing at 300 °C (see Ref. 9). After each treatment T_c was measured in a Quantum Design low-field superconducting quantum interference device (SQUID) magnetometer. In the first experiments, T_c was determined from dc magnetization measurements at 30 μT in 0.03 K steps on a time scale of about 3 min per step. However, after the following treatment steps flux pinning in the samples became more significant, and the unavoidable overshoot during temperature changes in the instrument led to a large difference in the T_c values deduced from the branches with increasing and decreasing temperature. Therefore, an unambiguous evaluation of T_c was impossible. In order to avoid the history effect involved in the dc measurements, the method had to be changed to measurements of the ac susceptibility at 30 μT, where the transition in the in-phase signal was observed. Also, the temperature ramp was slowed down by introducing additional 10 min breaks after each 0.03 K temperature step in the region of interest. The equivalence of the results deduced from the method with the previous experiments was carefully checked by extremely slow dc experiments, which then converged towards the values from the ac measurements. In that way, the hysteresis between the branches with increasing and decreasing temperature could be reduced to about 0.08 K, which allowed us to characterize the relative changes in T_c after each sample treatment with sufficient accuracy. The T_c values were always extracted from the magnetization data in increasing temperatures by evaluating the intersection between the tangents of the data in the normal conducting region and of the steepest slope in the in-phase ac signal.

In order to obtain information about flux pinning in the sample, magnetization data were measured after each treatment. They were collected in a noncommercial high-field S.H.E. SQUID magnetometer in fields up to 8 T. Most of the experiments consisted of field loops at constant temperature, from which the shielding currents were calculated by an extended Bean formalism,[17] which considers demagnetizing effects to first order. This formalism relies on the full flux penetration in the samples, and replaced the field-dependent currents in the sample by their average value. In this way, the time-dependent shielding currents were measured after a necessary waiting time of 10 min following each field change. By convention, I will denote these as the critical current densities J_c, which is probably appropriate for a relative comparison of results obtained from the same procedure, but has to be taken into account, if experiments with other time scales are to be compared. This static approach is also justified by the fact that discussions in the present paper depend on the functional dependence of J_c on B and the defect density, which are not significantly changed by relaxation (cf. Ref. 18).

Field loops at temperatures of 5 and $\sim$77 K were measured in order to obtain typical results for both the low- and high-temperature range. No change of the critical currents at 5 K is expected by the small changes of T_c after the sample treatments, but in order to avoid this additional influence at high temperatures, all the field loops at $\sim$77 K were made at the same reduced temperature $T/T_c = 0.838$, the ratio between 77 K and T_c of the untreated sample. In order to check the limited accuracy for setting the temperature (0.1 K) in our instrument, additional checks by varying the measure-

ment temperature by 0.1 K were made for one sample treatment. They did not show significant changes in the results.

For measurements with field orientations close to the ab planes, the reproducibility of the orientation is extremely important. The construction of the sample holder, as described above, can ensure a reproducibility to within 0.1°. At a certain stage, the sample holder broke during one experiment, which led to a reduced orientation reproducibility and made it impossible to evaluate the results for the magnetization measurements at $T=5$ K and $H_a \| ab$. However, the data at 77 K did reproduce to within a few percent after repeating the measurement with a new sample rod. Also, they were symmetrical and did not show any signs of misorientation, as for instance, a sudden increase of the magnetic moment at a certain field, or extremely large moments in decreasing external field. From this, the calculation of critical current densities at 77 K appears to be reliable.

The irreversibility lines (IL's) were estimated from the temperature-dependent magnetization at fixed external fields of 0.1, 1, 3, 5, and 7 T. They were determined by comparing the raw output data of the magnetometer, taken during the periodic sample movement. Due to relaxation effects and the inhomogeneity of the magnetic field ($\sim 10^{-3}$ %) different output voltages are observed at the same sample position, when the sample moves up and down, respectively. The sum of the squares of these differences (taken at each coordinate of the sample movement) is a characteristic parameter, and shows a very significant and sharp signature of the irreversibility line. At the irreversibility temperature, this ''hysteresis parameter'' abruptly goes to zero. If the merging point of the zero-field-cooled and field-cooled branches of the magnetic moment are considered, the IL is found at much lower temperatures, and is less well defined, in accordance with the longer time scales associated with this evaluation procedure (e.g., Ref. 19).

The sample was irradiated with neutrons in the central irradiation facility of the TRIGA reactor in Vienna (for a description of the neutron energy distribution see Ref. 20). In the reactor, the sample was sealed in a quartz container in air. The temperature during irradiation is around 60 °C, the irradiation time at full reactor power is 3 h 39 min for a fast neutron fluence of 1×10^{21} m^{-2} ($E>0.1$ MeV). After irradiation, the sample was left in the reactor for about one week, at a temperature of about 40 °C during reactor operation and at ambient temperature for the rest of the time. After that, the sample was stored at room temperature for times varying between two days and six weeks, depending on the availability of the magnetometers. Repetition of the measurements after extended storage times did not show any influence of room-temperature storage on the results.

III. DEFECT STRUCTURES

In our previous work, a strong interaction between the defect structure prior to irradiation and the radiation-induced defects was invoked to consistently explain the experimental data.[6] This qualitative picture is based on estimates of the defect mobility and the processes of defect creation. The role of oxygen in YBCO has been widely discussed. In standard single crystals an oxygen deficiency occurs, which leads to a small reduction of T_c compared to its maximum. Recently, this dependence of T_c on the oxygen deficiency δ was investigated down to $\delta=0$, where for small δ again a decrease of T_c from the maximum was observed. In standard crystals (like the one used in the present work) a reduction of the oxygen content always leads to a decrease in T_c, which indicates oxygen deficiency in the bulk of the material. Oxygen is quite mobile in YBCO at ambient temperature, which leads to a diffusion of defects in the sublattice. They may cluster or get caught by the strain field of a larger defect, which acts as a sink for mobile point defects. These larger defects are also present in YBCO single crystals, especially in the form of twin boundaries, or other growth defects like dislocations, stacking faults, etc. At elevated temperatures, the mobility of small defects is enhanced, clusters may dissolve, and only defect sinks with large strain fields will be able to trap them.

Under the neutron irradiation, a wide spectrum of defects is created in the crystal by elastic collisions of the neutrons with the atoms. Depending on the energy transferred from the neutron to the primary recoil atom, point defects or larger defect structures are created. In an avalanchelike process a huge number of atoms is displaced, leading to local melting of the crystal, and resulting in a spherical region of amorphous material with a mean diameter of $\sim$3 nm. These cascades have been thoroughly characterized by TEM,[4] where their concentration was found to be proportional to the neutron fluence, with a neutron mean free path of 20 cm before cascade production (i.e., 10^{22} m^{-3} cascades at a fast neutron fluence of 2×10^{21} m^{-2}, $E>0.1$ MeV). This ensures an isotropic distribution of the defects in the comparatively small single crystal. During the cascade process, a large number of high-energy atoms escapes from the cascade region into the surrounding crystal, which is also confirmed by the vacancy type of these regions, i.e., their inwardly directed strain field.[4] Oxygen, as the most mobile component in the system, is expected to contribute the largest fraction of these additional radiation generated interstitials. According to rough calculations of the defect mobility in the oxygen sublattice, most of these defects anneal even during irradiation or in a very short time afterwards.[21] The remaining defect structure determines the physical properties of the superconductor as observed in our experiments. Following the discussion above, a certain surplus of interstitials is expected in the bulk, at the expense of the depleted cascades, which will be relevant especially in the oxygen sublattice.

In the following annealing step, defect clusters can dissolve under thermal activation and point defects will diffuse through the crystal.[22] Compared to the preirradiation annealing, now large defect cascades exist, which are stable against annealing and will act as defect sinks. Concerning the distribution of small defects, the additional interstitials will be able to recombine with previously existing vacancies, which even leads to a reduction of defects in the bulk, again at the expense of the completely destroyed cascade regions.

IV. CRITICAL TEMPERATURE

Each sample state was characterized by measuring the critical temperature. The results as a function of the neutron fluence are shown in Fig. 1. For our analysis, we will use the value of T_c as the characteristic signature of the density of

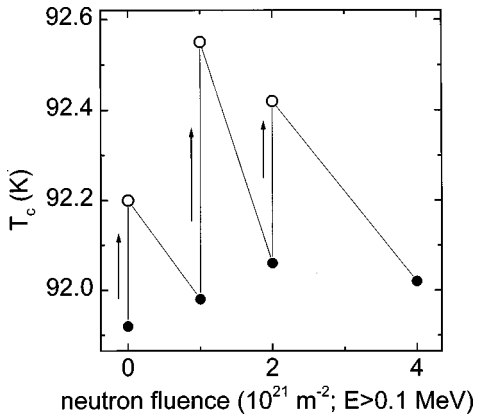

FIG. 1. The critical temperature T_c as a function of neutron fluence. Open symbols depict values after annealing, the arrows indicate the sequence of the treatments.

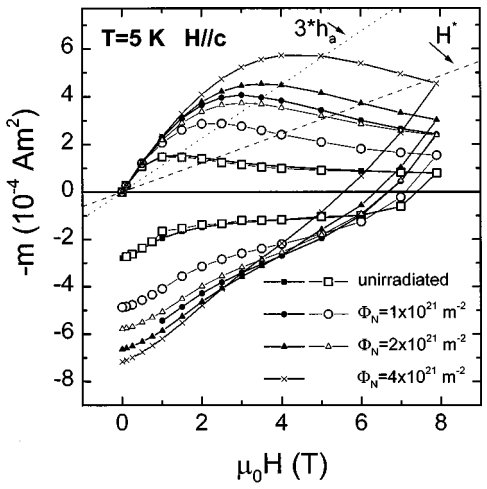

FIG. 2. Magnetic moments at $T=5$ K and $H_a \| c$. The dashed line shows the exact calculation of the Bean penetration field, the dotted line shows a more relaxed criterion, which allows for errors of a few percent in the calculation of J_c from the magnetization. Open symbols are the data after annealing for 8 h at 250 °C.

small defects in the crystal. This can be done because the defects in the oxygen sublattice will always be a significant fraction of all small defects, and they show the well-known sensitive correlation to T_c.[23] On this basis, the interpretation of the data in Fig. 1 is rather straightforward considering the defect dynamics discussed in the previous section. In the as-grown crystal, an unknown number of point defects exists in the oxygen sublattice, which leads to a slightly depressed T_c compared to a optimum-doped YBCO crystal.[23] In this context it should be noted that the absolute values of T_c in the present work are significantly higher than the optimum-doped samples in Ref. 23, which may be due to the small gold contamination of the crystal. During the first annealing step, clusters of interstitials dissolve, point defects are mobilized and are, with a certain probability, caught at defect sinks. This leads to a buildup of larger defects, and, at the same time, to a reduction of the point-defect concentration. Because the crystal is oxygen deficient, not all defects in the oxygen sublattice can be removed, which limits the increase of T_c.

During the irradiation process, the defect structure described in the previous section is introduced, which leads to a significant reduction of T_c. Upon annealing after the irradiation, some recombination of vacancies and interstitials as well as trapping of defects in sinks occur. Especially the oxygen distribution in the crystal is improved compared to the state before irradiation and annealing. The previously existing vacancies in almost the complete volume of the sample are saturated to some extent at the expense of a lowered oxygen content in the cascade regions. Only this model can explain the observed dependence of T_c on irradiation and annealing, and therefore appears to be correct.

Calculations of the defect dynamics were made[24] using a simplified model. These calculations consider the oxygen sublattice in a homogeneous system, i.e., the effect of twin boundaries and cascades is neglected. This is probably permissible in the case of the twin boundaries, as their density is very low compared to the defect concentrations we are interested in. The presence of the cascades, as described above, may probably not be neglected for both effects, i.e., for the additional creation of interstitials during the cascade process, and for the trapping of defects during annealing. Nevertheless, the calculations qualitatively reproduce the experimental data at low neutron fluences, where the influence of the cascades is not so important.

V. IN-PLANE CRITICAL CURRENT DENSITIES— $H_a \| c$

A. Experimental results

Once the variation of the small defect density is characterized by the T_c measurements, their effect on flux pinning has to be evaluated. Annealing leads to a removal of small defect structures, leaving only twin boundaries and defect cascades intact. In a previous experiment,[9] this was used to discriminate between the various contributions to flux pinning. The crystal was irradiated and subsequently annealed. The difference between the critical currents before and after annealing was attributed to the small defects, while the remaining critical current density after annealing was supposed to be due to the defect cascades. This interpretation depends on the linear superposition of the elementary pinning forces from all kinds of defects. Competitive or synergistic effects of the various defects are neglected. Therefore, in the present work a series of sequential irradiation and annealing experiments was chosen, in order to distinguish more exactly between the two contributions. In this experiment, the small defects formed during each irradiation step build up from (almost) zero after annealing, while the number of the stable defect cascades accumulates. It has to be mentioned that the expression ''small defects'' in this section addresses all defects that are (at least almost completely) removed by annealing, regardless of their actual size. Even large oxygen-deficient regions are microscopically invisible, but are strong pinning centers. These clusters can also be removed by annealing. Therefore, the actual size of the defects will be discussed in more detail in the next subsection.

From the dependence of the critical current densities on the irradiation and annealing processes, direct conclusions can be drawn about the mechanisms involved. The magnetization loops for $H_a \| c$ at low temperatures are shown in Fig. 2, the dashed straight line denotes the position of the Bean penetration field. For increasing fields, J_c cannot be evalu-

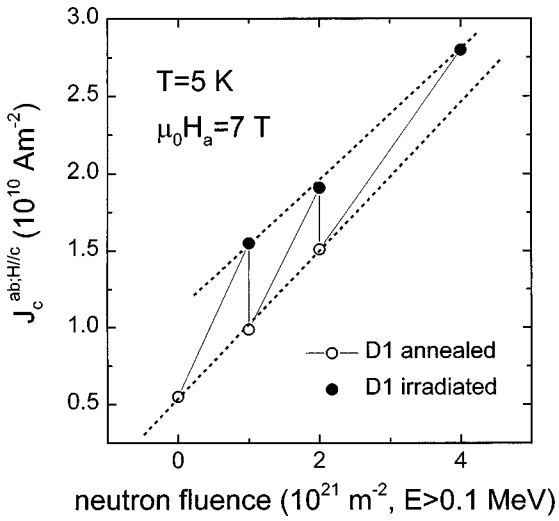

FIG. 3. Critical current density $J_c^{ab;H\|c}$ as a function of neutron fluence at $T=5$ K. Open symbols denote values after annealing of crystal $D1$.

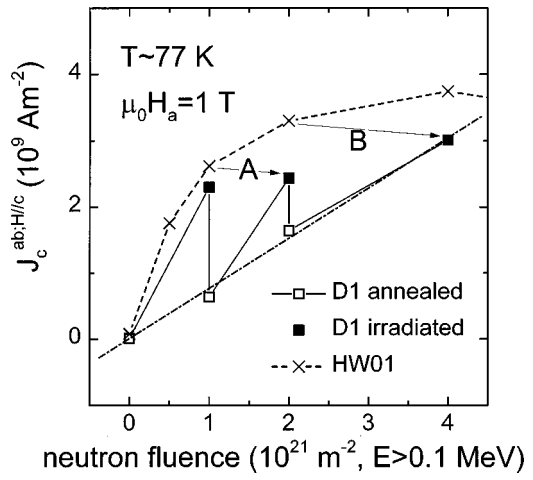

FIG. 4. Critical current density $J_c^{ab;H\|c}$ as a function of neutron fluence at $T\sim 77$ K. Open symbols denote values after annealing of crystal $D1$ (this work). For comparison, data on crystal HW01 from Ref. 6 are included. The arrows, marked A and B, link the corresponding measurements, if small defects dominate the flux pinning.

ated from data above this line in terms of a simple model based on an extended Bean formalism. The dotted line shows a more relaxed criterion, where a small error due to the logarithmic peak in the calculation of the penetration field is tolerated.[25]

After annealing only cascades and other large defects determine J_c, because no significant concentration of smaller defects is present. After irradiation, the combined effect of both, small and large defects, is visible. Due to the unknown mechanism of summation of the elementary pinning forces f_p to the experimentally observed macroscopic pinning force P_V, a clear separation is not possible. Figure 3 shows the in-plane critical current densities for $H_a=7$ T and $T=5$K, as evaluated from the magnetization loops for $H_a\|c$. This is the only field at $T=5$ K, where $J_c^{ab;H\|c}$ can be evaluated for all sample states from magnetization measurements by the extended Bean model. (If a small error of less than 5% due to the partial penetration is neglected, the data can also be evaluated down to $H_a=5$ T and lead to similar results.) A significant contribution of the large defects to the macroscopic pinning force is clearly visible from the increase of J_c after the second irradiation, but is not fully responsible for the observed critical current density, which can be seen by the significant decrease of J_c after annealing. With increasing significance of the cascade contribution a decreasing fraction of the critical current density can be related to the small defects. This is illustrated by the dotted lines in Fig. 3, where a clear decrease of the difference between the J_c values in the irradiated and annealed states is found with increasing neutron fluence.

Examples of the critical current density for $H_a=1$ T at $T\sim 77$ K are shown in Fig. 4. At this temperature the sample is penetrated by flux at almost all fields, which allows us to calculate J_c from the magnetization data for almost the complete accessible field range. The critical current density after the second irradiation is almost equal to that after the first. Because the cascades are twice as many after the second irradiation, their contribution to J_c has to be extremely small. This is illustrated by the comparison with a previous irradiation experiment without annealing. J_c of the crystal HW01 at a fast neutron fluence of 1×10^{21} m^{-2} (data from Ref. 2) is about the same as for crystal $D1$ (this study). If small defects determine flux pinning, the same value should be observed for the second irradiation of $D1$ after annealing. This is shown by arrow A in Fig. 4. After the third irradiation, the density of small defects in $D1$ should correlate to the additional neutron fluence, i.e., 2×10^{21} m^{-2}. Assuming that small (or invisible) defects determine J_c, this has to be similar to the current density of HW01 at this fluence, which is very well fulfilled (arrow B in Fig. 4).

The elementary pinning force due to core pinning is proportional to the intersecting volume of the defect and the vortex. If pinning by small defects (of the order to one nm) is assumed, their density would have to be very high, in order to yield a stronger effect than the larger cascades, which have roughly ten times larger elementary pinning forces. In this case, the force of the larger pins acting on the FLL would have to be less than their actual elementary pinning force, because the gradient in the FLL would already be stabilized by the large number of smaller defects. When the small defects are no longer able to support the macroscopic pinning force, the larger defects cannot hold this gradient either, because their number is too small, even if the elementary pinning force is very strong. The second possibility is, that the so-called ''small'' defects are actually large, but microscopically invisible. This would correspond to the existence of defect clusters, which are removed upon annealing. They will be discussed later on.

In both possible cases, more effective pinning by large defects can only be expected if the density of strong pinning centers is high enough. The onset of this regime around 77 K may occur at the third irradiation step (at a fast neutron fluence of 4×10^{21} m^{-2}). The J_c value now falls almost exactly on the linear extrapolation of the ''cascade contribution'' derived from the J_c values after annealing (dot-dashed line in Fig. 4), and also coincides with the expected contribution of small defects (arrow B in Fig. 4).

B. Summation models

A major task is the identification of the relevant summation process of the elementary pinning forces f_p to the mac-

roscopic pinning force $\mathbf{P_V} = -\mathbf{J_c} \times \mathbf{B}$. Few successful attempts for this summation exist, which can roughly be divided into two sections. The first is valid for strong elementary pinning forces, while the second, based on collective pinning, basically is only applicable to weak pinning forces.[26] The terms strong and weak pinning are, in this context, neither due to the absolute value of the elementary pinning force nor to the thermal stability of pinning, but to the relative maximum distortion u_0/a_0 the force causes in the flux-line lattice, where a_0 is the flux-line lattice parameter $1.07\ (\Phi_0/B)^{1/2}$.

In the group related to strong pinning, two approaches are commonly considered. The first is the direct summation, where the macroscopic pinning force is simply the sum of all elementary pinning forces, characterized by the average force f_p and the defect density N_d. This formalism neglects the influence of the flux-line lattice.

$$J_c \cdot B \approx N_d \cdot f_p . \tag{1}$$

If the influence of the flux-line lattice cannot be ignored, only one approach has been used for a strong pinning situation, i.e., the statistical dilute pinning summation,[27,28] which is thoroughly discussed in Ref. 29. The validity of this approach has been seriously questioned (e.g., Ref. 30) because of the obvious success of the collective-pinning model,[10] and especially because the ''pinning threshold,'' which defines the lower limit of f_p for effective pinning in the framework of the dilute pinning model. This parameter is inconsistent with experimental data. Nevertheless, the ''pinning threshold'' is only one feature of the model, and expresses the model's own limitations, but not those of the physics of flux pinning. Therefore, the theory may well be applicable in dilute strong pinning situations, i.e., with large local lattice distortions due to the pins, but without an overlap of these distortion fields from various pinning sites. The saturation or collective effects due to strongly overlapping strain fields cannot be described theoretically at present. The dilute pinning model gives

$$J_c B \approx N_d f_p^2 \left(\frac{u_0}{f_p} \right) \frac{d}{a_0^2}. \tag{2}$$

In this equation, the ratio u_0/f_p of the maximum distortion u_0 and the corresponding elementary pinning force describes the influence of the elasticity of the FLL. d is the range of the pinning force, typically of the order of ξ.

The group of weak pinning scenarios is based on the collective-pinning approach,[10] which has been significantly modified by various authors, leading to a broad range of expressions, which are widely used in literature. The basic approach is concisely presented in a review,[31] where the equations for the three-dimensional (3D) flux-line lattice

$$J_c B = 0.0039 \frac{N_d^2 f_p^4}{d^2 c_{66}^2 c_{44}}, \quad \text{(3D)} \tag{3}$$

and also for the 2D case of decoupled planes with thickness t

$$J_c B = 0.2 \frac{N_d f_p^2}{d\ t\ c_{66}}, \quad \text{(2D)} \tag{4}$$

are given. In these equations c_{66} and c_{44} are the elastic moduli of the flux (line) lattice for shear and tilt, respectively. In Ref. 30, these formulas are stated to describe the system for large correlation radii (large flux-line bundles), with a crossover to the direct summation, if the correlation radius decreases to the size of a_0.

A more complex approach is chosen in Ref. 32, where basically the same result for the regime of large flux bundles is achieved, but the presence of stronger pinning or weaker lattice potential leads to a ''small bundle'' regime and, finally to the ''single vortex pinning'' region. For reasons of compactness, the formulas are not given here, but will be considered only for the functional dependence of J_c on B and N_d in the following.

Because of the large number of material constants necessary for the calculations I will try to use only functional dependences, whenever possible. Nevertheless, especially for the calculation of the elastic constants of the FLL, a set of material parameters is needed, which is described in the following. The effective width of the pinning center d is calculated from $r_{\mathrm{def}} + \xi_{ab}$. For the calculations $\mu_0 H_c = 1\ T$, $\lambda_{ab}(t) = \lambda_{ab}(0)(1-t^2)^{-1/2}$ with $t = T/T_c$, and $\lambda_{ab}(0) = 140$ nm are assumed. The same temperature dependence is used for λ_c, with $\lambda_c(0) = 1.04\ \mu$m.[33] The elementary pinning forces are calculated from the product of the condensation energy density $\mu_0 H_c^2/2$ and the intersecting volume between the flux-line core of diameter ξ and the average spherical defect, with a cascade radius of 3 nm. This is a common procedure, but one has to be aware that the results are upper limits of more exact calculations. For $T = 5$ K an elementary pinning force of $f_p \approx 3 \times 10^{-12}$ N is obtained. This leads to a $u_0 \approx 3$ nm at 1 T, u_0 being roughly proportional to $B^{-1/2}$.

In a first step, the dependence of J_c on B is calculated according to the various models and compared with experiment. Due to the influence of thermal activation, which was not assessed in our experiments, the interpretation of the data has to be made in the framework of static pinning. In that way, a fraction of the defects with high pinning energy provide stable pinning, and will sustain the flux gradient after the comparatively long time before the measurement starts. This is only a first-order approximation, but justifiable in view of the other approximations made in the evaluation of the data. Since thermal activation corrections can be neglected at low temperatures, the analysis will start at 5 K. The critical current densities $J_c^{ab;H\|c}$ for various annealing and irradiation steps are shown in Fig. 5 as a function of B. The most interesting feature of the plot is the similarity of the curves, which will be discussed in the next subsection. At first, I will use the slope of the curves in an attempt to identify the responsible summation mechanism. The direct summation Eq. (1) follows a power law $J_c \alpha 1/B$, dilute limit summation, Eq. (2), gives roughly $B^{-0.5}$. The exponent is actually not a constant, but a consequence of the FLL contribution u_0/f_p, which is calculated from elastic theory[34] using the nonlocal elastic constants c_{11}, c_{44}, (Ref. 35) and c_{66}.[36] The limitation of the elastic theory to small distortions

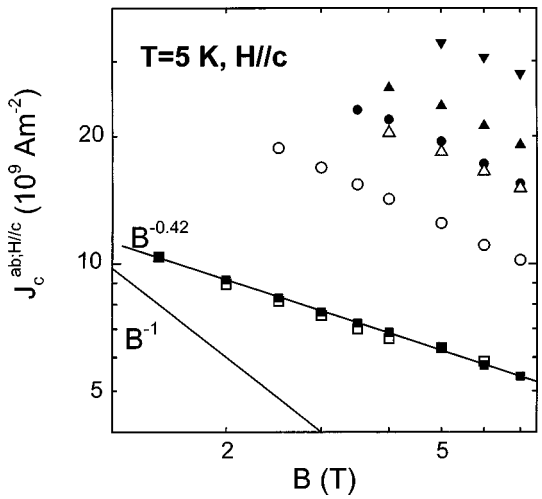

FIG. 5. Critical current density $J_c^{ab;H\|c}$ of crystal $D1$ as a function of the induction B at $T=5$ K. Open symbols denote values after annealing. Solid lines show the limiting cases of the slope, the dotted line is a fit to the dilute pinning summation, with a defect density enhanced by a factor of 100.

is not stringent (up to 0.5 a_0), because of the high nonlocality of the lattice. The same holds for the 3D collective approach, Eq. (3), which is roughly described by the exponent -3.75 (no exact calculations are available). The 2D collective-pinning approach, Eq. (4), yields the same dependence as the direct summation, i.e., $1/B$. The widely used collective-pinning approach from Ref. 32 gives three distinct contributions in the 3D regime, starting with the field-independent single vortex regime. A very wide range for the field dependence is mathematically possible in the small bundle regime, ranging from an increase proportional to B to an exponential decay of the form $\exp(-\text{const}\times B^3)$, but this regime is typically limited to very small field ranges. The large bundle pinning regime in this formulation is governed by a potential law B^{-3}. The 2D formalism in the approach of Ref. 32 features single pancake collective pinning, which again is field independent,[37] and a 2D collective-pinning region with $J_c \alpha 1/B$, corresponding to Eq. (4). For fields higher than a crossover field B_b^{3D}, three-dimensional collective pinning is predicted. Comparing all these equations with Fig. 5, the only reasonable explanation of the results can be found in the dilute limit statistical summation, Eq. (2).[38]

The same analysis was made for the defect density. As previously discussed, J_c after annealing the irradiated samples depends only on large, stable defects, which consist to the largest part of the radiation generated defect cascades. As their density is known to within a factor of unity (or may be slightly underestimated, cf. Ref. 4), the attempt to use the cascade density as the pinning center density seems feasible in this case. For $T=5$ K, an average elementary pinning force $f_p=3\times10^{-12}$ N ($r_{\text{def}}\lesssim 3$ nm), and a density of defects according to the TEM observations are assumed. In the statistical dilute limit summation, critical current densities are found, which are smaller than the experimental ones by a factor of 100. A fit including this factor of 100 to the data of the annealed sample at a neutron fluence of 2×10^{21} m^{-2} is shown as the dotted line in Fig. 5. This result is not very encouraging, in view of the fact that only this approach describes the field dependence of J_c. The calculated values could be enhanced by adjusting the parameters, but this also has some physical limits. One can assume a higher defect density than that deduced from TEM, which might yield in the ''best'' case a factor of 5. Additionally, the FLL may be softer than calculated, which could be feasible considering the layered character of the material and would lead to some reduction of c_{44}. Unfortunately, this possibility is very limited because the stability of the FLL to the creation of Frenkel pairs is proportionally weakened, which makes it impossible to increase u_0/f_p by more than a factor of ~ 3. The same argument holds for an increase of the elementary pinning force, which would have exactly the same effect. The last parameter that can be increased in Eq. (2) is the range of the pinning potential d, which is already set to rather generous 2.5 nm in the calculations above. Considering this, an overall factor of 15 could be gained by extending the range of material parameters slightly beyond the plausible values. This is still significantly below the factor of 100 missing between calculations and experiment.

Another attempt was made by introducing the 2D approach into the dilute pinning summation. u_0 was calculated under the condition $c_{44}=0$, and corrections for the elementary pinning force per pancake were made. Also, the defect density in this picture has to be increased by the number of superconducting planes intersecting a large defect (i.e., a maximum of three in our case). This approach did not improve the situation, but actually made the fit to the experimental data even worse. Therefore, the statistical dilute pinning approach cannot be considered to give satisfactory results for the summation of elementary pinning forces in our case.

In an attempt to improve the situation, the other theories were tested with respect to the defect density. As expected, the collective approaches did not even closely resemble the experimental results, especially because of the bad fit to the field dependence, and also because the experimental dependence of J_c on the defect density is linear rather than quadratic, as expected from the collective-pinning theory. Interestingly, the data for the sample after irradiation and annealing were well described by the direct summation, Eq. (1), at least for high fields above 5 T. The mismatch at low fields is given by the square root of the field, i.e., roughly a factor of 2.5 at $B=1$ T. This is by far better than the possible values using Eq. (2). Still, the field dependence of J_c differs significantly from the experimentally observed data.

The present theories cannot satisfactorily explain the observed dependence of $J_c^{ab;H\|c}$ on field and defect density. While collective approaches completely fail due to the presence of strong pinning forces, the available strong pinning theories are not able to consistently describe the experimental data. This seems to indicate a strong need for further theoretical investigation of the summation problem.

C. Weak vs strong pinning

The most prominent feature of Fig. 5 is the similarity between all the curves, disregarding whether the sample is untreated, or irradiated and/or annealed. Considering the expected defect structures in the sample, this behavior is worth a detailed discussion. Almost all present interpretations use the collective-pinning approach to describe flux pinning in HTSC's single crystals. This approach is based on the action of weak pinning centers, which have to be present at large

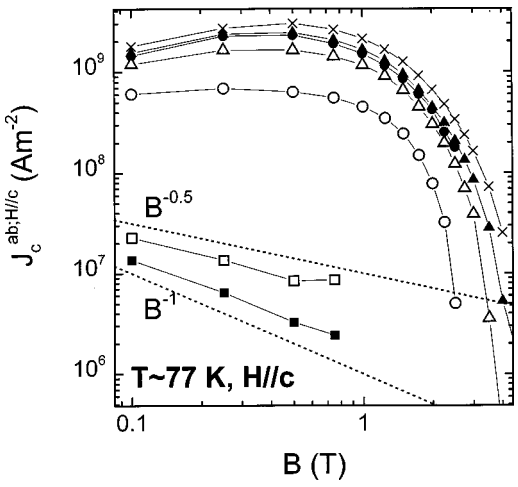

FIG. 6. Critical current density $J_c^{ab;H\|c}$ of crystal $D1$ as a function of the induction B at $T\sim 77$ K. Open symbols denote values after annealing.

densities to cause the experimentally observed current densities. The plausibility of this approach has often been shown, also for YBCO [beginning in 1991 (Ref. 39)].

For the sample used in this study, however, it was shown, that the present summation theories do not explain the critical currents at low temperature. On the other hand, the pinning centers after annealing the irradiated sample, are well identified to be the defect cascades. The pinning action of these defect cascades is certainly strong, as they distort the FLL by up to a few tenths of the lattice parameter a_0. Consistently, the strong pinning summation models are able to explain at least some features of the data. On the other hand, the same field dependence of J_c for all sample states is a clear signature that all states are subject to the same summation model. This implies that strong pinning *always* prevails in our sample, even if it is neither annealed nor irradiated.

A marked effect of neutron irradiation on the functional behavior of J_c vs B is only visible at 77 K (Fig. 6). Thermal activation certainly cannot be neglected in the following discussion of this dependence. Nevertheless, the following discussion is based on a static picture, as discussed previously. In this approach, the decayed shielding currents, after the time set by the experiment, are interpreted in the framework of a critical state model.

In the as-grown and annealed state, the first data points up to 1 T follow a power-law behavior with $J_c \alpha B^{\beta}$, similar to that for $T=5$ K (Fig. 5). In the as-grown sample the exponent β is close to -1 (direct summation), after annealing it changes to -0.6 (consistent with dilute statistical summation), which is in both cases some indication for strong pinning, similar to the discussion of the low-temperature data. For higher fields the resolution of our experimental setup is reached. The J_c values of the irradiated sample, though, increase with B in low fields, and decrease extremely fast after a peak. This fishtail behavior is not discussed in detail in the present paper, although I would like to point out that explanations depending on the creation of new pinning centers in oxygen-deficient regions do not seem to be convincing in the presence of the strongly pinning cascades, which are normal conducting at all temperatures. For all measurements on annealed samples, the currents are much higher than in the untreated sample. If the fishtail is to be explained by properties of the defect structure, it is extremely difficult to find the same explanation for the very different defect structures of many unirradiated crystals[40] and irradiated samples, which have J_c values larger by more than an order of magnitude. Therefore, I favor interpretations of the fishtail effect in terms of properties of the flux-line lattice. In the present work, the fishtail is not observed in the unirradiated sample, but develops as a consequence of the radiation.[41] On the other hand, the defect cascades which are responsible for a large part of pinning in the irradiated samples, are certainly strong pinning centers with distortions of the FLL of the order of $u_0/a_0\sim 0.25$. Therefore, interpretations of the fishtail effect in terms of collective-pinning models are not supported by the present data.

The critical current density in the unirradiated sample at high temperature is extremely low, and the magnetization curve actually looks reversible for almost the complete experimental field range. Still, the field dependence strongly resembles that at low temperature, which has been identified as strong pinning. From the very low J_c values, a rather high quality of the present crystal can be deduced, which is much better than that of many crystals for which weak pinning has been assumed. As strong pinning has been shown to describe the data of the present crystal, collective pinning in standard YBCO single crystals has to be seriously questioned. If this also applies to very high quality detwinned crystals available now, will have to be checked separately. The nature of the strong pinning centers will also have to be investigated further. Consistent with recent work,[42,43] the assumption of oxygen clusters in the vicinity of stable lattice defects seems to be plausible in the context of the defect mobility, on which the present work depends. These clusters could be large enough to cause strong pinning ($\gtrsim$1 nm), are microscopically invisible, and can dissociate during annealing. Therefore, they could well be responsible for pinning, also in clean standard YBCO single crystals. If, and to which extent twin boundaries could be candidates for this type of defect, will also be the scope of further studies.

VI. OUT-OF-PLANE CRITICAL CURRENT DENSITIES— $H_a\|ab$

Because of the experimental problems with the sample orientation, which were already discussed in the Sec. II, only experiments at $T\sim 77$ K are considered in this section. The critical current density $J_c^{c;H\|ab}$ as a function of fast neutron fluence is shown in Fig. 7. In contrast to the data for the other field orientation, a clear increase of J_c is observed after the second irradiation, which proves the relevance of the large defects for flux pinning in this geometry. After the third irradiation, the critical current density decreases to that after the first irradiation. If the data are compared to the experiment on the crystal HW01,[6] we find that $J_c^{c;H\|ab}$ in the older crystal is lower by almost an order of magnitude, although the size of the in-plane current densities is comparable in both crystals. Obviously, huge sample-to-sample variations exist, which will be tentatively explained in the following.

After annealing, the current densities drop by almost one order of magnitude. Therefore, the large defects were initially supposed to be ineffective for that field direction.[9] The

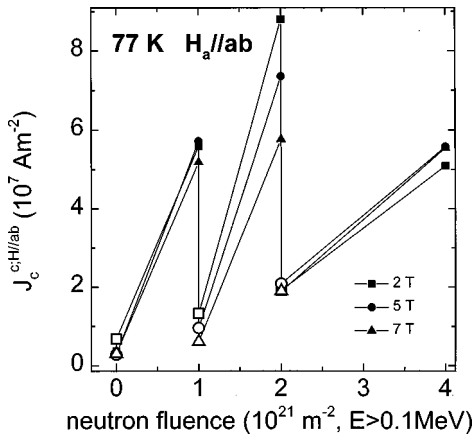

FIG. 7. Critical current density $J_c^{c;H\|ab}$ as a function of neutron fluence at $T\sim 77$ K. The open symbols denote values after annealing.

significant increase after annealing and reirradiation (almost a factor of 2 after the second irradiation) proves, however, the importance of the large defects.

The observed effects can be explained consistently by the qualitative approach developed in Ref. 6, which is confirmed by the present experiments. Flux lines in the direction parallel to the ab planes are heavily influenced by the anisotropy of the material. The magnetic-field distribution is dominated by the two different λ values in and across the planes, leading to an elliptical shape of the flux line. Assuming an anisotropic superconductor, this also causes anisotropic elastic moduli of the flux line lattice. Especially the tilt modulus is significantly harder for bending the flux lines out of the planes than for in-plane deformations. Another important factor is the modification of the flux-line core by the anisotropic coherence length ξ, which leads to an elliptic core, with the short axis ξ_c perpendicular to the CuO_2 planes, and the long axis ξ_{ab} parallel to the planes. On the other hand, the description in terms of an anisotropic superconductor is not sufficient, because it does not include the layered structure of the material, which additionally changes the flux-line geometry. The order parameter between the planes is significantly lower than in the plane, which leads to the well-known intrinsic pinning effect. No details about the resulting local variations of ξ and λ are available, but generally larger values than the experimentally determined averages are expected between the planes. A consistent treatment is only available for two-dimensional systems, where the flux-line cores between the planes vanish, resulting in Josephson vortices.[44] This may be relevant for YBCO at low temperatures, but is not expected in the high-temperature regime around 77 K, to which the experiments discussed in this chapter refer.

The consequences for flux pinning in the geometry $H_a\|ab$ are quite important. On one hand, the intrinsic pinning effect strongly pins the vortices against movements across the CuO_2 planes, which is important in transport measurements (e.g., Ref. 45), where the critical current density $J_c^{ab;H\|ab}$ is measured. In magnetic measurements, this quantity is usually not accessible, because the smaller critical current density $J_c^{c;H\|ab}$, describing the sliding of the flux lines along the planes, limits the magnetic moment. Flux lines in this field direction are forced in between the CuO_2 planes by the intrinsic pinning effect. At this site the superconducting order parameter is very low, or even close to zero, which implies a strongly reduced condensation energy and a large ξ, both of which reduce the pinning force for this sliding motion. If flux pinning due to a defect of a specific size is considered, we automatically obtain a huge anisotropy of the measured critical current densities for the two field directions, $J_c^{ab;H\|c}$ and $J_c^{c;H\|ab}$. For the case $H_a\|c$ the flux lines have to cross the CuO_2 planes, where the full local condensation energy in a volume ($\sim r_{\mathrm{def}}^2\xi_{ab}$ for small defects) has to be supplied, causing comparatively strong flux pinning. The described movement of flux lines for $H_a\|ab$ is only hindered by the strongly reduced pinning force from the same defect (cf. Fig. 1 in Ref. 6). This reduction strongly depends on the size of the order parameter between the planes, e.g., on how close the superconductor is to two-dimensionality. In a two-dimensional system, no core pinning effect is possible for Josephson vortices. Therefore, a tiny increase of the order parameter between the planes can strongly enhance the observed critical currents by introducing core pinning. This effect is important for the addressed difference in $J_c^{c;H\|ab}$ between the older crystal HW01 and $D1$ of the present work. While the values of $J_c^{ab;H\|c}$ of the unirradiated crystal $D1$ are much smaller at 77 K (indicating the higher quality of the crystal due to a lack of large defects) and comparable after irradiation, $J_c^{c;H\|ab}$ is almost an order of magnitude larger in crystal $D1$. The magnetization for $H_a\|c$ is relatively independent of variations in the interlayer order parameter, because each flux line sees the average of all positions perpendicular to the layers, while a strong influence of this parameter can be expected for flux lines parallel to the layers. This implies that the newer crystal $D1$ is more three-dimensional in character than the older HW01. At first sight this seems quite implausible, as the layers in the higher quality crystal should be better defined. An explanation of the data can be based on a study of the layered structure of YBCO as a function of charge-carrier density,[46] where the authors conclude, that by optimum doping of YBCO the CuO chains become superconducting, i.e., the interplanar order parameter is significantly enhanced. These considerations have been supported by specific-heat measurements,[23] which show a strong increase of the specific-heat jump $\Delta C(T_c)/T_c$ with increasing oxygen concentration. From a comparison of the T_c values and from the almost reversible magnetization curves at 77 K and $H_a\|c$ in crystal $D1$, one may conclude that the doping is better than in HW01, leading to a higher interplanar order parameter with the described effects on flux pinning for $H_a\|ab$.

The interplanar order parameter can also be changed by the scattering of the conduction electrons by defects in the crystal. The anisotropy is due to the electronic mass tensor, the Fermi surface, and the electron-phonon coupling. By isotropic scattering of the electrons some fraction of the anisotropy can be removed, leading to a smearing of the layered structure of the superconducting properties. The in-plane maximum of the order parameter will be slightly reduced, but at the same time the interplanar minimum will be increased. Due to the small absolute value of the interplanar order parameter small changes in the anisotropy will induce

a relatively large increase of the minimum, which enhances the pinning properties for $H_a \| ab$.

This mechanism is responsible for the effect of irradiation and annealing on $J_c^{c;H\|ab}$. For this field direction, small defects are comparatively useless for flux pinning, due to the reduced order parameter between the planes. By isotropic scattering, though, they increase the interplanar order parameter, and thereby enhance the pinning effect of the large defects. After annealing, the small defects are removed, the maximum anisotropy of the system is restored, and therefore, the interplanar order parameter becomes minimal again, which in turn minimizes the flux-pinning effect of the large defects. With the next irradiation step, new large defects are introduced, and also a large number of small defects, which reduce the anisotropy, and enable flux pinning by the cascades.

Another interesting feature is observed in the dependence of $J_c^{c;H\|ab}$ on the fluence. We find a distinct maximum after the second irradiation, and a significant decrease afterwards. The maximum of J_c with increasing defect density has also been observed in the experiment on HW01, but at significantly higher fluences. It was interpreted as an overloading of the lattice with pinning centers. The flux-line lattice attempts to accommodate optimally to the defect structure, but this attempt is limited by the internal lattice forces. If too many defects are present, they will have a competing effect on the flux lines, leading to a decreased macroscopic pinning force $\mathbf{J_c} \times \mathbf{B}$. Especially under the influence of thermal activation the critical currents will decrease rapidly, because of the resulting low-energy separation between the possible pinning configurations. Why this effect occurs much faster in crystal $D1$ than in HW01, can also be seen from considerations of the interplanar order parameter. Due to the intrinsic pinning effect, the flux lines are confined to their positions between the CuO_2 planes. Adaption to the array of pinning centers, therefore, is only probable by bending parallel to the planes, which is governed by the corresponding elastic constant c_{44}. This elastic constant is highly dispersive and decreases (approximately proportional to λ_c^{-2}) with the interplanar penetration depth. At present further calculations are impossible, because the local λ_c values in the interplanar regions are unknown. Obviously, they should lie between the measured average values for this direction and the corresponding Josephson penetration length if two-dimensionality is assumed. The possible variation of λ_c is, therefore, quite large and may well explain the change in the stiffness of the flux lines against bending. The higher interplanar order parameter in the crystal $D1$ leads not only to higher elementary pinning forces and a higher $J_c^{c;H\|ab}$, but also to less flexible flux lines. This feature initially increases J_c for low defect densities, but also causes an earlier saturation of the macroscopic pinning force with increasing density of pinning centers.

In Fig. 8, the very weak field dependence and comparable size of $J_c^{c;H\|ab}$ at neutron fluences of 10^{21} m^{-2} and at 4×10^{21} m^{-2} prior to annealing, is compared to the higher values at 2×10^{21} m^{-2}, which show a much stronger variation with field.

In a slightly speculative approach, this behavior may be attributed to two different situations for flux pinning. In the first, where a low density of pinning centers is present, each pinning center holds more than one vortex (over some bending length of the flux lattice), because the intrinsic pinning effect makes the flux-line cores queue up between the CuO_2 planes. If the elementary pinning force is strong enough, the intrinsic pinning force may be the limiting factor. In this case, flux lines move around a pinned one in a shear mechanism. During this movement, they have to cross the intrinsic pinning barrier, which will lead to a field independent J_c, if the average angle, at which the flux lines cross the barriers, is field independent. If the pin density roughly matches the flux-line density (again divided by the bending length), pinning may be higher than allowed by the intrinsic contribution. For higher pin densities, the competitive effect of the different pinning centers leads to a reduction of effective pins, and again to a limitation by intrinsic pinning. The consistency of this approach is supported by a comparison with the data on HW01. As mentioned before, the difference in $J_c^{c;H\|ab}$ between the two crystals can be explained by a higher interplanar order parameter in the higher-quality crystal $D1$. This implies a higher intrinsic pinning effect in HW01, but also a much weaker elementary pinning force of the defects. Consistently, $J_c^{c;H\|ab}$ in this crystal is limited only by f_p and is not field independent for any defect density.

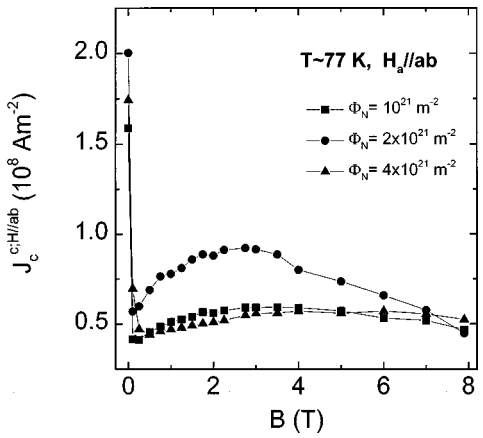

FIG. 8. Critical current density $J_c^{c;H\|ab}$ as a function of the induction B for the sample after irradiation and prior to annealing.

Presently, the question for the physical reason of the specific fishtail shape of $J_c^{c;H\|ab}(B)$ has to be left unanswered, if the matching argument considered above cannot be supported. Again, the cause of the pinning anomaly has to be a feature of the FLL, and not of the defect structure of the sample, in order to be consistent with the observed J_c values. Defects caused by oxygen deficiency cannot dominate pinning for one specific fluence value and be less efficient below and above.

VII. IRREVERSIBILITY LINES

The irreversibility line is a parameter often used to describe high- T_c superconductors for technical purposes. Various techniques can be employed for its assessment (e.g., Ref. 19), which lead to comparable results under the careful observation of the characteristic time scales and resolution of the experimental quantity. Considering the irreversibility line

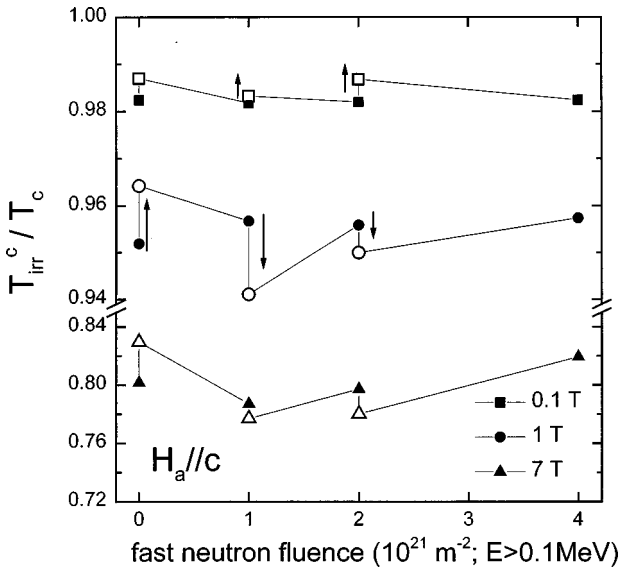

FIG. 9. Reduced irreversibility temperatures for $H_a = 0.1$, 1, and 7 T parallel to the c direction as a function of neutron fluence. The open symbols denote values after annealing.

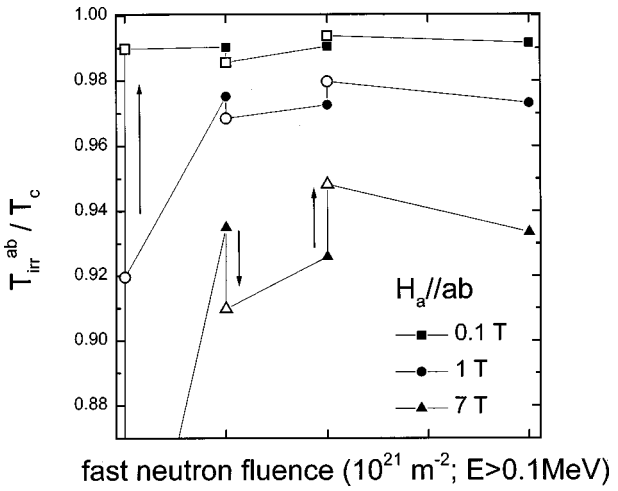

FIG. 10. Reduced irreversibility temperatures for $H_a = 0.1$, 1, and 7 T perpendicular to the c direction as a function of neutron fluence. The open symbols denote values after annealing.

(IL) as a measure for the stability of pinning against thermal activation, it should be possible to consistently explain the data with the previously developed model. Figure 9 shows the reduced irreversibility temperature $t_{\rm irr}^{c} = T_{\rm irr}^{c}/T_c$ as a function of the fast neutron fluence for some fields applied parallel to the c axis. The data for the lowest field, 0.1 T, depend predominantly on changes of T_c, which are scaled away by the reduced temperature. Because of the closeness of T_c, the interpretation of these data in terms of flux pinning is not simple due to the additional strong influence of the reversible properties. The increase of H_c at high temperatures, for example, can be responsible for the increase of $t_{\rm irr}^{c}$ after annealing. In general, $t_{\rm irr}^{c}$ is shifted up with the first annealing step prior to irradiation. This can be interpreted by the movement of small defects into defect sinks, where they create larger pinning centers, which support thermally stable flux pinning. The decrease of $t_{\rm irr}^{c}$ after the first irradiation step is consistent with the removal or weakening of a large portion of these defects (O vacancies) after the cascade process, while the density of the introduced cascades is still too low to allow thermally stable flux pinning. With increasing neutron fluence, the defect density, and with it $t_{\rm irr}^{c}$, increases. After annealing, $T_{\rm irr}^{c}$ decreases for all fields above 1 T, consistent with a removal of smaller and medium-sized defect clusters. A decreasing size of the cascade areas could also be involved, as the clusters of small defects situated in the strained regions close to the cascade can move to the amorphous central region and release some of the inwardly directed strain. Substantially more data at intermediate neutron fluences would be necessary for a more detailed analysis.

Figure 10 shows the reduced irreversibility temperatures $t_{\rm irr}^{ab}$ for the field direction $H_a \| ab$. This parameter was very small for the untreated sample. After the first annealing treatment, a huge increase is found, probably also due to the clustering of smaller defects. Following neutron irradiation $t_{\rm irr}^{ab}$ again increases significantly. Consistently with the critical current measurements, $t_{\rm irr}^{ab}$ develops a peak at the second fluence 2×10^{21} m^{-2}. The most remarkable feature in this data set is the change in $t_{\rm irr}^{ab}$ after annealing. While annealing after the first irradiation reduces $t_{\rm irr}^{ab}$, it is strongly enhanced by annealing after the second neutron irradiation. Two counteracting processes connected with the reduction of the interplanar order parameter occur during annealing. The first is the decrease of the elementary pinning force, which is the dominating process for annealing after the first irradiation, and the second is the softening of the flux lines, which is relevant for dense pinned centers after the second irradiation. In this way a consistent explanation of the observed effects can be found. Considering the low number of relevant data points the significance of this explanation still needs further confirmation. In order to decide if the approach is valid, a number of experiments at additional neutron fluences between 10^{21} and 2×10^{21} m^{-2} are necessary.

VIII. CONCLUSIONS

Reactor neutron irradiation has been used to introduce additional defect structures into a YBCO single crystal. Part of this defect structure, the large defect cascades, is well characterized in size and concentration by TEM. These defects are large enough to cause significant local distortions in the flux-line lattice and, therefore, act as strong pinning centers. Little is known about the other defects in the system, which are TEM invisible. It has been shown experimentally and is also expected from theoretical considerations, that point defects and a large fraction of clusters can be removed by annealing at $T = 250$ °C. Therefore, after annealing, only the large defect cascades are left in the sample (beside twin boundaries, which have a comparatively weak effect on flux pinning and few other thermally stable defects). This is also confirmed by the radiation- and annealing-induced variation of T_c. After irradiation and subsequent annealing, T_c is significantly enhanced due to the recombination of the previously existing oxygen vacancies and the interstitials created during the cascade process. A slow decrease of T_c during the experiments is due to a buildup of stable defects.

After annealing, a well-defined defect structure prevails in

the samples, which allows an analysis in terms of elastic theory. In a first step, various summation models were tested in order to explain the critical current densities for $H_a \| c$ as a function of field and the defect density. Consistent results for the defect density could only be achieved from the direct summation. The field dependence $J_c^{ab;H\|c}(B)$ at $T=5$ K did not show the corresponding $1/B$ dependence, but followed a power law B^{β} with an exponent $\beta \sim -0.5$. This power law is characteristic of the statistic dilute pinning summation, which cannot explain the dependence on defect density, which leaves us without a consistent theoretical explanation of the results.

The power law $B^{-0.5}$ for $H \| c$ and at $T=5$ K is not changed by any sample treatment, but is observed at all experimental steps. This infers a similar mechanism for the summation of elementary pinning forces in all these sample states, even though flux pinning is supposed to be dominated by the strongly pinning defect cascaded after annealing and by the TEM invisible defects after irradiation. If the invisible defects were causing weak pinning, they would have to follow a different summation (e.g., collective pinning), which is obviously not the case. Therefore, strong pinning at various defect densities is found to prevail in the sample.

At high temperatures close to 77 K, the field dependence of J_c also follows a power law with β between -0.6 and -1 for the sample before irradiation. After irradiation another type of behavior is always present, which does not follow a power law, but a distinct fishtail maximum. From the similarity of the power law with the low-temperature case, strong pinning is also highly plausible at high temperatures. Pinning after irradiation is not weakened, and therefore, the fishtail behavior seems to be a flux-line lattice effect caused by strong pinning.

The data for $H_a \| ab$ confirm our model for anisotropic flux pinning in layered superconductors. The layered structure of the superconductors pins the flux lines intrinsically between the superconducting CuO_2 planes, but at the same time reduces the condensation energy at this location. This effect severely limits the available elementary pinning forces. Only large pinning centers can, therefore, contribute to flux pinning in this field direction. The elementary pinning force in this case is not only due to the size of the defect, but also to the order parameter between the planes, which is a function of the material anisotropy. A high anisotropy is equivalent to a low order parameter between the planes and low pinning forces. The anisotropy of the system can be reduced by isotropic scattering of the electrons by small defects, which enhances the order parameter between the CuO_2 planes. In that way, flux pinning for $H_a \| ab$ is due to the large defects, but is enhanced strongly by the presence of a large number of small defects. After annealing the small defects are removed and the pinning effect of the cascades is drastically reduced. After an additional irradiation, new cascades are created and the flux pinning of all large defects is again enhanced by the newly introduced small defects. The intrinsic pinning effect in this field direction additionally improves the efficiency of each pinning center by allowing the queuing-up of more than one flux line behind each defect. This leads to a dramatic increase of the IL in this field direction even at the first (small) neutron fluence of 10^{21} m^{-2}. At the highest neutron fluence (4×10^{21} m^{-2}), the density of pinning centers is too high due to the intrinsic pinning effect and the FLL cannot adapt to all defects. The resulting competitive effect of the defects on the FLL reduces the macroscopic pinning force, especially in the presence of thermal activation.

If the elementary pinning forces are strong enough and the density of these pinning centers is not optimal, $J_c^{c;H\|ab}$ can be limited by the intrinsic pinning effect. From the treatment dependence (annealing/irradiation) of the data, one can infer that the fishtail effect for this field direction also has to be a property of the flux-line lattice and is not due to additional defects, which become activated by increasing the field.

In summary, neutron irradiation and annealing of YBCO single crystals was used to explore many basic features of flux pinning. The conclusions for $H_a \| c$ presented here, indicate that a careful analysis has to be made before applying collective-pinning theory to YBCO single crystals. They support the interpretation of the fishtail effect in terms of a flux-line lattice property and not by a significant change in the defect structure due to a change in the external field. The data for $H_a \| ab$ fully support the model, according to which the elementary pinning force is controlled by the small defects in the sample. The small defects change the interlayer order parameter by isotropic scattering of the electrons.

ACKNOWLEDGMENTS

I wish to thank M. A. Kirk and G. W. Crabtree, MSD, Argonne National Laboratory, for providing the crystal. Numerous helpful discussions with them and with all my colleagues from the Superconductivity Group of the Atominstitut headed by H. W. Weber, and especially with M. Werner, are thankfully acknowledged. My special thanks go to Yu. V. Trushin, St. Petersburg, for long and helpful discussions on the defect mobility in YBCO superconductors.

[1] H. W. Weber, F. Nardai, C. Schwinghammer, and R. K. Maix, Adv. Cryog. Eng. **22**, 329 (1982).

[2] R. Meier-Hirmer, H. Küpfer, and H. Scheurer, Phys. Rev. B **31**, 183 (1985).

[3] A. Umezawa, G. W. Crabtree, J. Z. Liu, H. W. Weber, W. K. Kwok, L. H. Nunez, and C. H. Sowers, Phys. Rev. B **36**, 7151 (1989).

[4] M. C. Frischherz, M. A. Kirk, J. Farmer, L. R. Greenwood, and H. W. Weber, Physica C **232**, 309 (1994).

[5] F. M. Sauerzopf, H. P. Wiesinger, W. Kritscha, H. W. Weber, G. W. Crabtree, and J. Z. Liu, Phys. Rev. B **43**, 3091 (1991).

[6] F. M. Sauerzopf, H. P. Wiesinger, H. W. Weber, and G. W. Crabtree, Phys. Rev. B **51**, 6002 (1995).

[7] J. Giapintzakis, W. C. Lee, J. P. Rice, D. M. Ginsberg, I. M. Robertson, R. Wheeler, M. A. Kirk, and M.-O. Ruault, Phys. Rev. B **45**, 10 677 (1992).

[8] L. Civale, A. Marwick, M. W. McElfresh, T. K. Worthington, A. P. Malozemoff, F. Holtzberg, J. R. Thompson, and M. A. Kirk,

Phys. Rev. Lett. **65**, 1164 (1990).
[9] B. M. Vlcek, H. K. Viswanathan, M. C. Frischherz, S. Fleshler, K. Vandervoort, J. Downey, U. Welp, M. A. Kirk, and G. W. Crabtree, Phys. Rev. B **48**, 4067 (1993).
[10] A. I. Larkin and Yu. N. Ovchinnikov, J. Low Temp. Phys. **34**, 409 (1979).
[11] H. P. Wiesinger, F. M. Sauerzopf, H. W. Weber, H. Gerstenberg, and G. W. Crabtree, Europhys. Lett. **20**, 541 (1992).
[12] B. M. Vlcek, M. C. Frischherz, S. Fleshler, U. Welp, J. Z. Liu, J. Downey, K. G. Vandervoort, G. W. Crabtree, and M. A. Kirk, Phys. Rev. B **46**, 6441 (1992).
[13] D. Markowitz and L. P. Kadanoff, Phys. Rev. **131**, 563 (1963).
[14] D. L. Kaiser, F. Holtzberg, B. A. Scott, and T. R. McGuire, Appl. Phys. Lett. **51**, 1040 (1987).
[15] Grown by B. W. Veal, and selected by Beatrix Vlcek, Argonne National Laboratory.
[16] Ch. Böhmer (unpublished).
[17] H. P. Wiesinger, F. M. Sauerzopf, and H. W. Weber, Cryogenics **203**, 121 (1992).
[18] M. Werner, F. M. Sauerzopf, H. W. Weber, A. Hoekstra, R. Surdeanu, R. J. Wijngaarden, R. Griessen, and K. Winzer, in *Critical Currents in Superconductors*, edited by T. Matsushita and K. Yamafuji (World Scientific, Singapore, 1996), p. 203.
[19] M. C. Frischherz, F. M. Sauerzopf, H. W. Weber, M. Murakami, and G. A. Emel'chenko, Supercond. Sci. Technol. **8**, 485 (1995).
[20] H. W. Weber, H. Böck, E. Unfried, L. R. Greenwood, J. Nucl. Mater. **137**, 236 (1986).
[21] Yu. V. Trushin (private communication).
[22] D. V. Kulikov, R. A. Suris, Yu. V. Trushin, V. S. Kharlamov, and D. Tsigankov, Tech. Phys. Lett. **22**, 920 (1996).
[23] V. Breit, P. Schweiss, R. Hauff, H. Wühl, H. Claus, H. Rietschel, A. Erb, and G. Müller-Vogt, Phys. Rev. B **52**, 15 727 (1995).
[24] F. M. Sauerzopf, M. Werner, H. W. Weber, R. A. Suris, D. V. Kulikov, V. S. Kharlamov, and Yu. V. Trushin, Physica C **282-287**, 1333 (1997).
[25] In terms of the reduced variables in Ref. 24, the value of 3^*h_a is chosen as a criterion, which gives a very small correction (on the order of $\sim$3%) of the magnetization compared to that at the correct value of the reduced penetration field h^* (cf. Fig. 3 of Ref. 24). Therefore, the resulting influence of these errors on the J_c values can be neglected.
[26] Extensions of the collective approach for columnar and planar defects as summarized in Chap. 9 of Ref. 32 are not applicable for the point forces considered in the present paper.
[27] K. Yamafuji and F. Irie, Phys. Lett. **25A**, 387 (1967).
[28] R. Labusch, Cryst. Lattice Defects **1**, 1 (1969).
[29] A. M. Campbell and J. E. Evetts, *Critical Currents in Superconductors* (Taylor and Francis, London, 1972), p. 115.
[30] E. H. Brandt, Rep. Prog. Phys. **58**, 1465 (1995).
[31] Which is confirmed by numerical calculations, F. M. Sauerzopf (unpublished).
[32] G. Blatter, M. V. Feigel'man, V. B. Geshkenbein, A. I. Larkin, and V. M. Vinokur, Rev. Mod. Phys. **66**, 1125 (1994).
[33] A. Porch, J. R. Cooper, D. N. Zheng, J. R. Waldram, A. M. Campbell, and P. A. Freeman, Physica C **214**, 350 (1993).
[34] E. H. Brandt, J. Low Temp. Phys. **26**, 709 (1976).
[35] A. Sudbo and E. H. Brandt, Phys. Rev. Lett. **66**, 1781 (1991).
[36] V. G. Kogan and L. J. Campbell, Phys. Rev. Lett. **62**, 1552 (1989).
[37] It remains unclear, which type of pinning center should collectively pin a single pancake.
[38] An attempt to use the wide adaptability of the 3D small bundle regime from Ref. 32 was not successful, because the variations in the slope of Fig. 5 are by far too strong to provide reasonable fits, even if the applicable range of the formula is extended far beyond its theoretically established value.
[39] C. J. van der Beek and P. H. Kes, Phys. Rev. B **43**, 13 032 (1991).
[40] M. Werner, Ph.D. thesis, Technical University, Vienna, 1997.
[41] In Ref. 40, the inverse behavior is observed very often, i.e., the fishtail is found prior to irradiation and is removed after irradiation.
[42] H. Küpfer, A. A. Zhukov, A. Will, W. Jahn, R. Meier-Hirmer, T. Wolf, V. I. Voronkova, M. Kläser, and K. Saito, Phys Rev. B **54**, 644 (1996).
[43] A. Erb, J.-Y. Genoud, F. Marti, M. Däumling, E. Walker, and R. Flükiger, J. Low Temp. Phys. **105**, 1033 (1996).
[44] J. R. Clem, Phys. Rev. B **43**, 7837 (1991).
[45] R. M. Schalk, H. W. Weber, Z. H. Barber, P. Przyslupsky, and J. E. Evetts, Physica C **199**, 311 (1992).
[46] J. L. Tallon, C. Bernhard, U. Binninger, A. Hofer, G. V. M. Williams, E. J. Ansaldo, J. I. Budnick, and Ch. Niedermayer, Phys. Rev. Lett. **74**, 1008 (1995).